ACS NANO

www.acsnano.org

ARTICLE

Full-Color Plasmonic Metasurface Holograms

Weiwei Wan, Jie Gao,* and Xiaodong Yang*

Department of Mechanical and Aerospace Engineering, Missouri University of Science and Technology, Rolla, Missouri 65409, United States

Supporting Information

ABSTRACT: **Holography is one of the most attractive approaches for reconstructing optical images, due to its capability of recording both the amplitude and phase information on light scattered from objects. Recently, optical metasurfaces for manipulating the wavefront of light with well-controlled amplitude, phase, and polarization have been utilized to reproduce computer-generated holograms. However, the currently available metasurface holograms have only been designed to achieve limited colors and record either amplitude or phase information. This fact significantly limits the performance of metasurface holograms to reconstruct full-color images with low noise and high quality. Here, we report the design and realization of ultrathin plasmonic metasurface holograms made of subwavelength nanoslits for reconstructing both two- and three-dimensional full-color holographic images. The wavelength-multiplexed metasurface holograms with both amplitude and phase modulations at subwavelength scale can faithfully produce not only three primary colors but also their secondary colors. Our results will advance various holographic applications.**

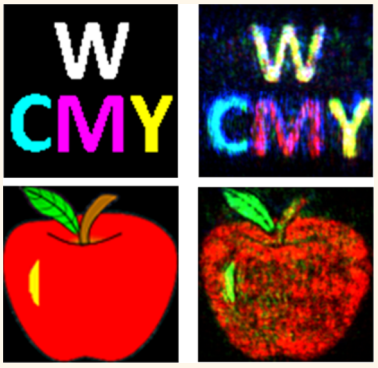

KEYWORDS: *metasurface holograms, plasmonics, full-color holography, 2D and 3D holography, wavelength-multiplexed encoding method*

A hologram contains the complete amplitude and phase information on light scattered from the original object and it can generate two- and three-dimensional (2D and 3D) optical images observed by the naked eye.[1] Conventional holograms rely on light propagation over distances much longer than the wavelength in order to accumulate enough phase change for wavefront shaping, resulting in the large size of optical components to build the hologram. Recently, optical metasurfaces made of subwavelength nanoantenna arrays in thin metallic films have provided an efficient way for manipulating the wavefront of light with well-controlled amplitude, phase, and polarization beyond the diffraction limit.[2−12] Metasurfaces have been designed to demonstrate versatile applications in optical vortex beam generation,[2,13−15] broadband quarter-wave or half-wave plates,[16−19] ultrathin flat lenses,[7,20,21] spin-hall effect of light,[22] and holographic imaging.[23−29] The optically thin holograms made of metasurfaces, so-called meta-holograms, enable us to engineer the spatial distributions of amplitude and phase of light with subwavelength resolution, providing the reconstructed holographic images with enhanced space-bandwidth product, high resolution, and wide field of view.[8,23] However, most of the existing metasurface holograms have only been designed to achieve holographic images with single color[23] or limited primary colors,[25,27,29] which greatly limit the performance of meta-holograms to reproduce 3D complex full-color images.

The major challenge for realizing color meta-holograms is how to independently record and reconstruct the amplitude and phase information on different color components. One approach is to utilize a large-size pixel consisting of several subpixels to record different color components.[27−29] This method is usually limited to two colors,[27,28] and it will introduce not only design complexity but also large pixel size with degraded imaging resolution if more color components are recorded.[29] Moreover, the existing color meta-holograms are designed to record only amplitude or phase information. Amplitude-modulated color holograms have been demonstrated by utilizing surface plasmon resonances,[24] metallic nanoparticle scattering,[27] and metamaterials fishnet transmission.[28] A phase-modulated multicolor hologram based on aluminum nanorods has also been demonstrated.[29] The quality of the images reconstructed from these color meta-holograms becomes degraded due to the loss of either amplitude or phase information. In the phase-only hologram design, although the random initial phase added to the point sources constituting the object can make the amplitude more uniform in the hologram plane,[23] the reconstructed image is inevitably accompanied by speckle noise. Therefore, the capability of recording both the amplitude and phase information on light scattered from the object is desirable in designing meta-holograms for yielding faithful optical images with low noise.[25]

In this work, we design and demonstrate ultrathin full-color plasmonic metasurface holograms with both amplitude and

Received: August 12, 2016
Accepted: September 21, 2016
Published: September 21, 2016

DOI: 10.1021/acsnano.6b05453
ACS Nano 2016, 10, 10671−10680

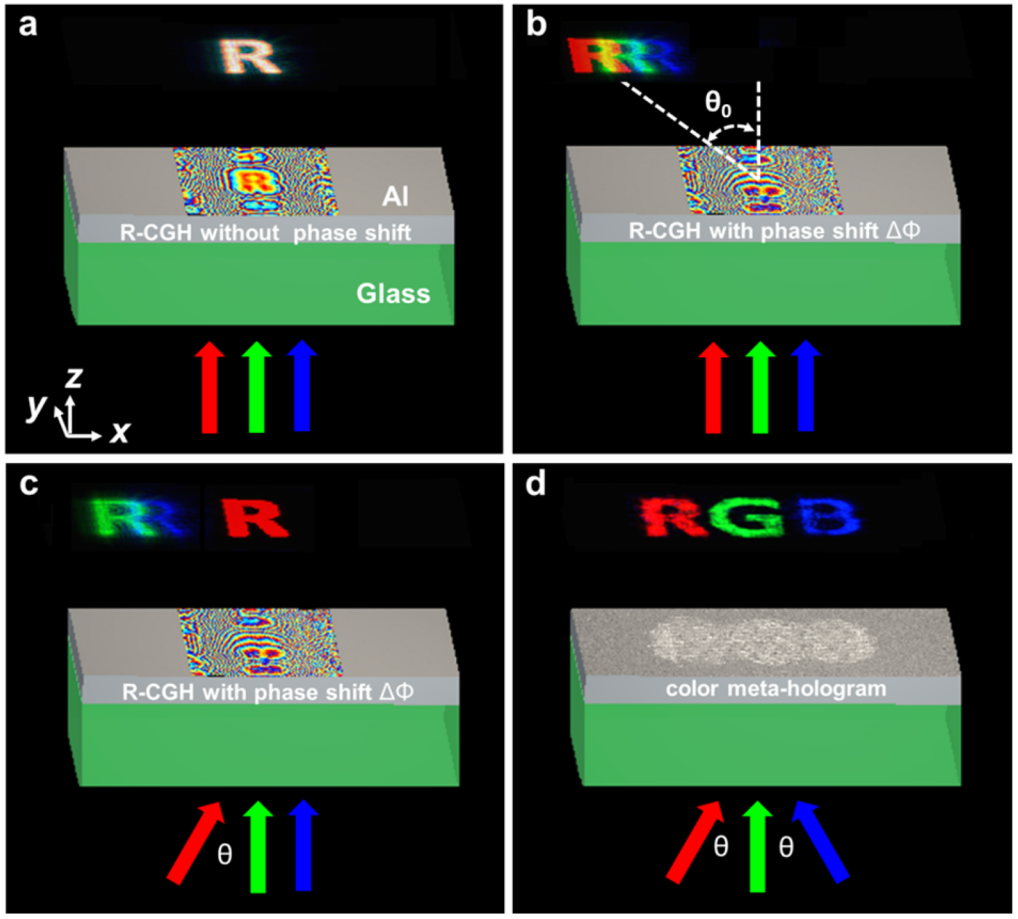

Figure 1. Design of a wavelength-multiplexed hologram for color "RGB" letters (red "R", green "G", and blue "B"). (a) Red-component computer generated hologram (R-CGH) without phase shift illuminated by normally incident RGB light. (b) R-CGH with additional phase shift ΔΦ illuminated by normally incident RGB light. (c) R-CGH with phase shift ΔΦ illuminated by normally incident green and blue light but tilted incident red light. Note that in panels a−c, the CGH patterns and the holographic images projected above the CGHs are the simulated results. (d) Measured 2D color holographic image produced by the fabricated metasurface holograms in aluminum film with normally incident green light but tilted incident red and blue light.

phase modulations for reconstructing 2D and 3D holographic color images with low noise and high quality. The metasurface holograms with subwavelength pixels are created by a wavelength-multiplexed encoding method[30,31] to record and reconstruct both 2D and 3D full-color optical images. Not only three primary colors (red, green, and blue, RGB in short) but also their secondary colors (cyan, magenta, yellow, and white, CMYW in short) can be reconstructed with high fidelity. We use geometric metasurfaces consisting of subwavelength nanoslits with spatially varying orientations in aluminum thin film to reproduce the computer-generated holograms (CGHs). The geometric phase[32,33] (Pancharatnam−Berry phase) feature of the designed metasurface hologram ensures that the spatial phase distribution is only determined by the orientation angle of the nanoslit, which is robust against fabrication tolerances and variation of material properties. In addition, our approach can provide clean reconstructed full-color holographic images by automatically filter out the desired color images and remove the unwanted side images from the optical setup.

RESULTS AND DISCUSSION

In order to design a wavelength-multiplexed metasurface hologram working for three primary colors (red, 633 nm; green, 532 nm; blue, 420 nm), we first set a virtual color object floating above the hologram plane and divide its color into RGB components. Each color component can be considered as many self-illuminating point sources at the corresponding single wavelength. By using a CGH algorithm, both the recording and the image reconstruction procedures do not require a reference beam. On the basis of the Huygens−Fresnel principle, the CGH of each color component (R-CGH, B-CGH, and G-CGH) can be individually calculated by superimposing the optical wave fronts from all the point sources.

Because the geometric metasurfaces for reproducing the CGHs work in broad bandwidth, the CGH of each color component will simultaneously generate color images for all three primary colors at the same position. To solve this issue, we encode an additional phase shift into the CGH of each color component and introduce the corresponding tilted incident angle illumination to reconstruct the desired color images. As an example, we consider 2D color letters "RGB" as the virtual object (red "R", green "G", and blue "B", as shown in Figure 1) and only take its red-color component with the R-CGH shown in Figure 1a, which records the diffraction pattern of red "R" letter. When the R-CGH is normally illuminated with red, green and blue light, the red "R", green "R" and blue "R" will be simultaneously reconstructed above the hologram and overlap to each other for generating a blurry white "R" letter. Because

DOI: 10.1021/acsnano.6b05453
ACS Nano 2016, 10, 10671−10680

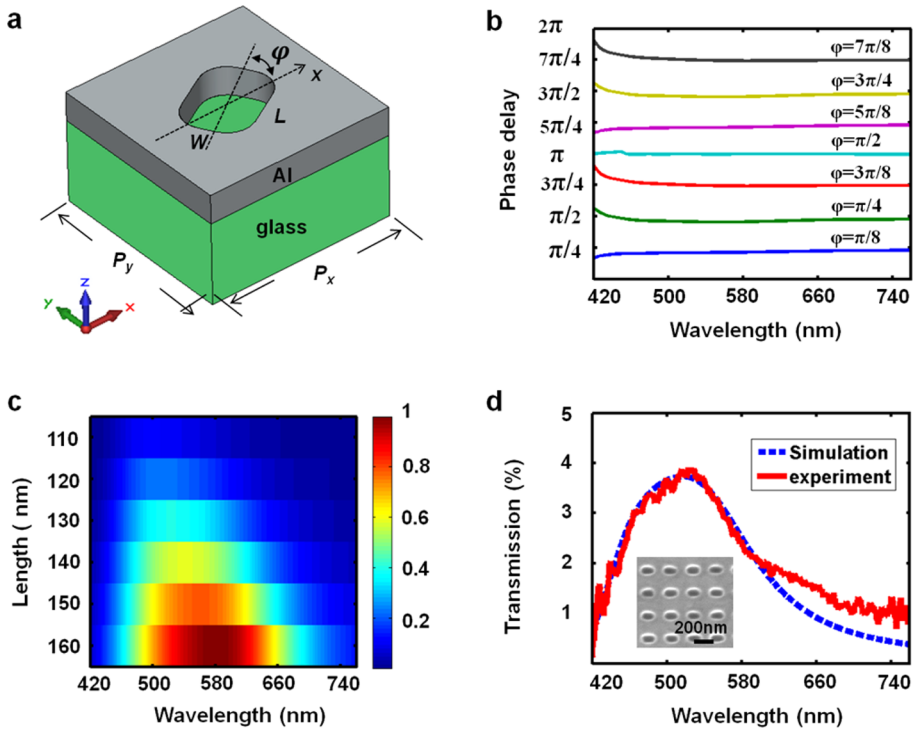

Figure 2. Nanoslit unit cell structure and its functionality for controlling phase delay and transmitted amplitude independently. (a) Geometry of the designed nanoslit unit cell structure representing one pixel in the metasurface hologram, with periodicity $P_x = P_y = 230$ nm. The thickness of aluminum film is $H = 35$ nm. The nanoslit have length $L = 160$ nm and width $W = 80$ nm, and it can rotate in the x-y plane with an orientation angle φ. All sharp corners of the nanoslit are smoothened out by cylindrical surfaces with a radius of 30 nm. (b) The simulated phase delay for different nanoslit orientation angles (with respect to the phase delay of the orientation angle $\varphi = 0$). (c) Simulated cross-polarization transmission spectra for nanoslits with different lengths. The transmission is normalized by the maximum intensity. (d) Comparison between the simulated and measured cross-polarization transmission spectra from the uniform nanoslit array. The fabricated sample is shown in the inset SEM image.

of the dispersion, only the designed red "R" image is focused, and the green and blue "R" images are blurry. Thus, this R-CGH cannot independently reconstruct red color separated from green and blue colors. The same cases will also occur for G-CGH and B-CGH. In order to enable the CGH of each color component to separate its own color from other colors, an additional phase shift $\Delta\Phi = -k_\lambda \sin(\theta_\lambda)\Delta x$ along the x axis is encoded into the CGH, where $k_\lambda = 2\pi/\lambda$, λ is the wavelength of each color component, θ_λ represents the incident angle of light at each color which is tilted along the x axis. The phase shift $\Delta\Phi$ introduces gradient phase change to the original R-CGH so that the reconstructed images for all three primary colors will be projected with an refraction angle of $\theta_0 = -\arcsin[k_\lambda \sin(\theta_\lambda)/k_0]$ as shown in Figure 1b, where k_0 is the wavevector of the reconstructed light. More illustration can be found in Supporting Information Figure S1. The reconstructed red "R" image can be shifted back to the position right above the hologram by compensating the phase shift $\Delta\Phi$ with a tilted incident angle θ_λ for the red light (as shown in Figure 1c). By introducing the additional phase shift into the hologram (encoding in the recording process) and the corresponding tilted incident angle illumination (decoding in the reconstruction process), the desired image with the right color can be correctly projected above the hologram (with the detailed theoretical analysis shown in Methods). Another factor influencing the quality of reconstructed image is the color dispersion in full-color holography, which will result in the different sizes of the reconstructed images for three primary color components. Here, the numerical zero-padding technique[30,34,35] (see Methods) is utilized to eliminate the color dispersion. Then, the CGHs of all three color components are synthesized into one combined hologram by the superposition of their complex amplitudes. At last, the phase of every pixel on the hologram is changed to the opposite sign because light propagates in the opposite direction during the recording and reconstruction processes. As shown in Figure 1d, the color "RGB" letters are finally reconstructed using a tilted incident angle illumination configuration, where the incident angles for red, green and blue light are set as 35°, 0°, and −35°, respectively.

The full-color metasurface hologram is created by substituting all the pixels on the CGH with nanoslits having various orientation angles in a 35 nm-thick aluminum film on a glass substrate. Aluminum is chosen due to its optical response covering the entire visible spectrum, which is essential for the realization of full-color meta-holograms. Figure 2a shows a unit cell of nanoslit with period $P_x = P_y = 230$ nm. The nanoslit has length $L = 160$ nm and width $W = 80$ nm, and it can rotate in the x−y plane with an orientation angle φ. Here, we consider the abrupt phase change that occurs for circularly polarized light converted to its opposite helicity. The transmitted light through a meta-hologram consists of two circular polarization states: one has the same handedness as the incident circularly polarized light (copolarization) without any phase delay, and the other has the opposite handedness (cross-polarization) but with a phase delay. This geometric phase delay Φ, known as Pancharatnam−Berry phase, is solely determined by the orientation angle φ of the individual nanoslit ($\Phi = \pm$

DOI: 10.1021/acsnano.6b05453
ACS Nano 2016, 10, 10671−10680

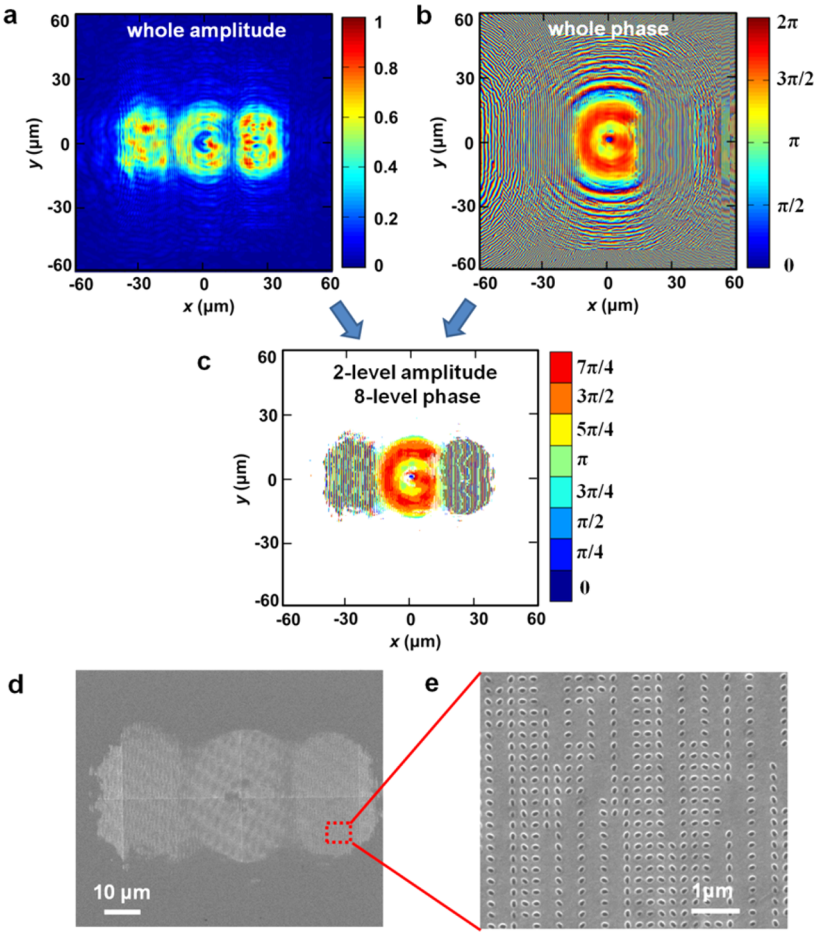

Figure 3. Two-amplitude and eight-phase modulations of a metasurface hologram for 2D color "RGB" letters. (a) Simulated amplitude distribution. (b) Simulated phase distribution. (c) Discrete eight-level phase distribution with a two-level amplitude modulation. (d), (e) SEM images of the fabricated metasurface hologram.

2φ),[32,33] where the sign "+" and "−" represent the phase delay for the incident left-handed and right-handed circular polarizations (LCP and RCP), respectively. Figure 2b shows the phase delay Φ with respect to the nanoslit orientation angle φ simulated by CST Microwave Studio software (see Methods). The relation of $\Phi = 2\varphi$ maintains well in broad bandwidth covering the wavelength from 420 to 760 nm, although a weak coupling between neighboring nanoslits introduces a small phase deviation when the wavelength is close to 420 nm. The averaged deviation of the simulated phase from the designed value is about $\pi/45$ and it is much less than the phase step of $\pi/4$ used in our hologram design. The influence of the nanoslit orientation angle on the amplitude deviation is also negligible (as illustrated in Supporting Information Figure S2). The dispersionless feature of the geometric phase controlled by the nanoslit orientation angle allows the designed meta-hologram to work in the entire visible spectrum. Moreover, by properly varying the nanoslit length, the geometric phase change still maintains but the optical transmission intensity from the nanoslit can be tuned (as shown in Figure 2c). Therefore, our designed meta-holograms made of nanoslits with various orientation angles and different lengths have the potential to control the amplitude and phase of light simultaneously and independently. In Figure 2d, the simulated and measured cross-polarization transmission spectra of the nanoslit shown in Figure 2a is plotted in the visible range, giving the transmission around 2%, 4%, and 1% for red, green, and blue light, respectively. According to the simulation results of the influence of nanoslit orientation angle on the transmission (as illustrated in Supporting Information Figure S2), the averaged transmission of the nanoslit arrays with eight orientation angles from 0 to π is about 1.2%, 3.5%, and 0.5% for red, green, and blue light, respectively, which is slightly lower than the transmission from the nanoslit array with zero orientation angle as plotted in Figure 2d. The inset of Figure 2d gives the scanning electron microscopy (SEM) image of the fabricated uniform nanoslit array. The optical setup for measuring cross-polarization transmission from the nanoslit array is described in Methods. More information about the copolarization transmission spectra and the optical field $|E|$ distributions in the nanoslit can be found in Supporting Information Figure S3.

Figure 3a,b shows the calculated spatial amplitude and phase distributions of the hologram designed for color "RGB" letters with the dimension of 120 μm × 120 μm, containing 512 × 512 pixels with the period P = 230 nm. The distance between the hologram plane and the virtual object is D = 110 μm. For simplicity, we only consider two-amplitude and eight-phase modulations to demonstrate the full-color meta-hologram here. We first modulate the whole amplitude distribution (as shown in Figure 3a) to get a two-level amplitude matrix. The amplitude modulation is achieved by two states of on and off with a chosen threshold, by setting a pixel with or without the nanoslit. The amplitude modulation threshold is set to be 0.2 ×

DOI: 10.1021/acsnano.6b05453
ACS Nano 2016, 10, 10671−10680

A_{max} (where A_{max} is the maximum of all of the amplitudes). The amplitudes smaller than the threshold are modulated to be zero, whereas other amplitudes are modulated to be one. Then we modulate the whole phase distribution (as shown in Figure 3b) to get an eight-level phase matrix. The phase map is modulated by using eight discrete phase levels between 0 and 2π (0, $\pi/4$, $\pi/2$, $3\pi/4$, π, $5\pi/4$, $3\pi/2$, $7\pi/4$) represented by identical nanoslits with eight orientation angles within the unit cells. Figure 3c shows the final discrete phase map using two-level amplitude and eight-level phase modulations, which is obtained by the multiplication of the two-level amplitude matrix and the eight-level phase matrix. The blank area in the discrete phase map shown in Figure 3c indicates the pixels without nanoslits so that the amplitudes are set to be zero and there is no phase modulation, whereas the pixels with amplitudes equal to one are assigned with the eight-level phase values. It is noted that the amplitude-modulation will reduce the overall transmission through the hologram and decrease the optical efficiency, although it improves the imaging quality by reducing the speckle noise. In our design, there is around 80% of the converted light transmitted through the hologram according to the filling ratio of nanoslits in the hologram, which is determined by the amplitude modulation threshold. Then the final estimated optical efficiency (the optical power ratio between the holographic image and the incident light) for our designed meta-hologram will be around 1.0%, 2.8%, and 0.4% for red, green, and blue light, respectively. The final dimension of the meta-hologram for color "RGB" letters is reduced into around 80 μm × 50 μm. The designed meta-hologram is then fabricated in a 35 nm-thick aluminum film deposited on a glass substrate using electron-beam deposition. The nanoslit arrays with lattice constant of $P_x = P_y = 230$ nm and nanoslit dimension of $L = 160$ nm and $W = 80$ nm are milled in the aluminum film according to the designed orientation angles using focused ion beam. Figure 3d,e shows the SEM images of the fabricated meta-hologram for color "RGB" letters. It is noted that the fabricated meta-holograms has compact microscopic sizes of less than 100 μm. The subwavelength features of the nanoslits ensure high spatial resolution for the hologram even with the microscopic size, which is important for many holographic applications such as high-density imaging processing and big data storage. Furthermore, the size of the holographic image region is determined by $R = \lambda \times D/P$, where λ is the wavelength of the reconstructed light, D is the distance between the holographic image and the metasurface hologram, P is the pixel size on the hologram. For the current design, the constructed holographic image has a microscopic size of around 250 μm. Actually, the size of the holographic image R can be enlarged by increasing the distance D in the CGH design with the meta-hologram of microscopic size. In practice, the large-size holographic images in centimeter scale can be obtained so that the image can be directly projected onto a plane and seen by the naked eye. Another point is that the resolution of a holographic image is determined by the pixel size of the image $R/N = (\lambda \times D)/(N \times P)$, where N is the pixel number. Regarding the design of the color "RGB" letters with $N = 512$, $D = 110$ μm, and $P = 230$ nm, the resolution of the holographic image (as shown in Figure 4b,c) is about 590 nm for the red light with $\lambda = 633$ nm.

Figure 4 shows the original 2D object (color "RGB" letters) together with the simulated and measured color holographic images reconstructed from the meta-holograms. The simulated holographic image displayed in Figure 4b is obtained by collecting the emission from all the point sources (*i.e.*, pixels) on the meta-hologram. The details of the optical measurement setup are described in Methods. In Figure 4b, it clearly shows that the desired images of color "RGB" letters are numerically reconstructed in the central region, which are well separated from the unwanted side images. Usually, one can pick up the desired central image by using a spatial filter, but it is not necessary in our optical setup. Taking the "G" letter as an example, the unwanted red and blue "G" images are projected on the reconstruction plane with angles of $\theta = \pm 35°$ (Figure 4b). However, the objective lens with a numerical aperture (NA) of 0.4 in the setup only allows to collect light within the angle less than 24°. As a result, the unwanted side images will not be captured by the CCD camera, and only the directly projected green "G" image at $\theta = 0°$ can be visualized in experiment (Figure 4c). By choosing the proper incident angles of light and NA of an objective lens, our optical setup can automatically filter out the desired color images. This spatial filtering mechanism is also verified by observing the unwanted side images once another objective lens with a larger NA of 0.8 is used. On the other hand, Figure S5 (see Supporting Information) shows the simulated color holographic image by using an eight-level phase modulated CGH without the amplitude modulation. It is clearly seen that the color of each letter suffers granular noise, that is, speckle noise. However, by using the CGH with both two-level amplitude and eight-level phase modulations, the color distribution of the reconstructed holographic images (as shown in Figure 4b) is uniform without speckle noise. The experimentally reconstructed holographic image (as shown in Figure 4c) also shows uniform color for each letter. The results indicate that the two-level amplitude modulation together with the eight-level phase modulation is sufficient enough to suppress the speckle noise that usually exists in the phase-only holograms without the amplitude modulation.

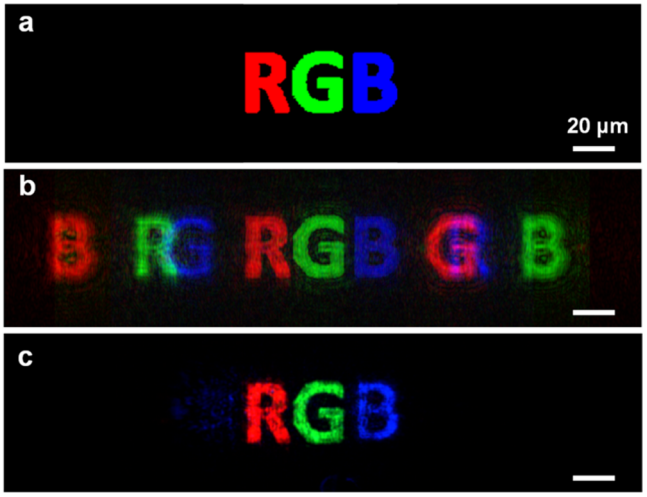

Figure 4. Original 2D object compared with the simulated and experimentally reconstructed color holographic images. (a) Original object of color "RGB" letters. (b) Simulated color holographic images. The central desired images are well separated spatially from the side images. (c) Experimentally reconstructed color holographic images from the fabricated metasurface hologram shown in Figure 3d, with the unwanted side images automatically filtered out by the objective lens with a certain NA. The original, simulated, and measured images almost have the same size.

DOI: 10.1021/acsnano.6b05453
ACS Nano 2016, 10, 10671−10680

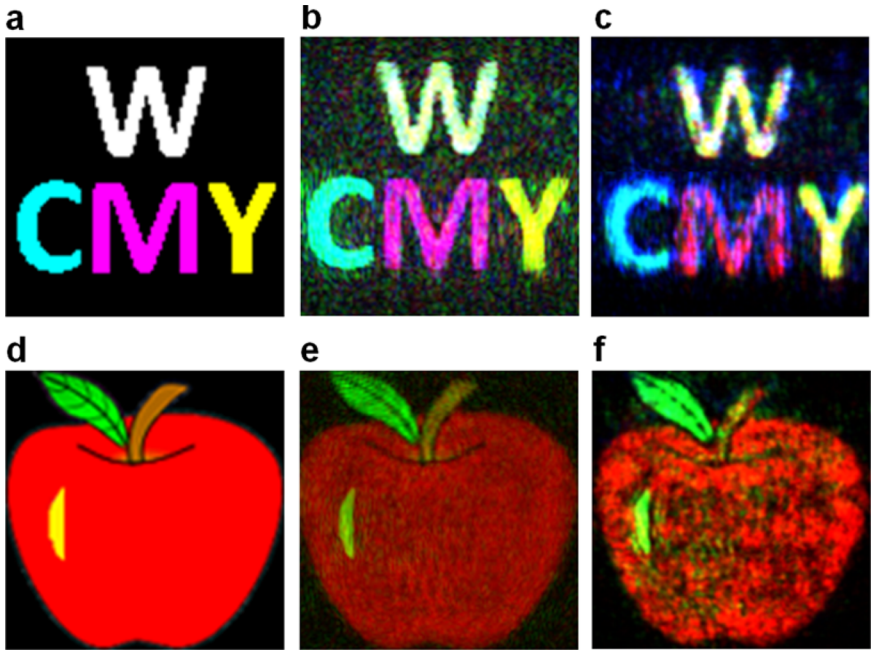

Figure 5. Reconstruction of 2D holographic images containing three primary colors and their secondary colors. (a) Original 2D object of color "CMYW" letters. (b), (c) Simulated and experimentally reconstructed holographic images. (d), (e), (f) Original apple object and its simulated and measured holographic images.

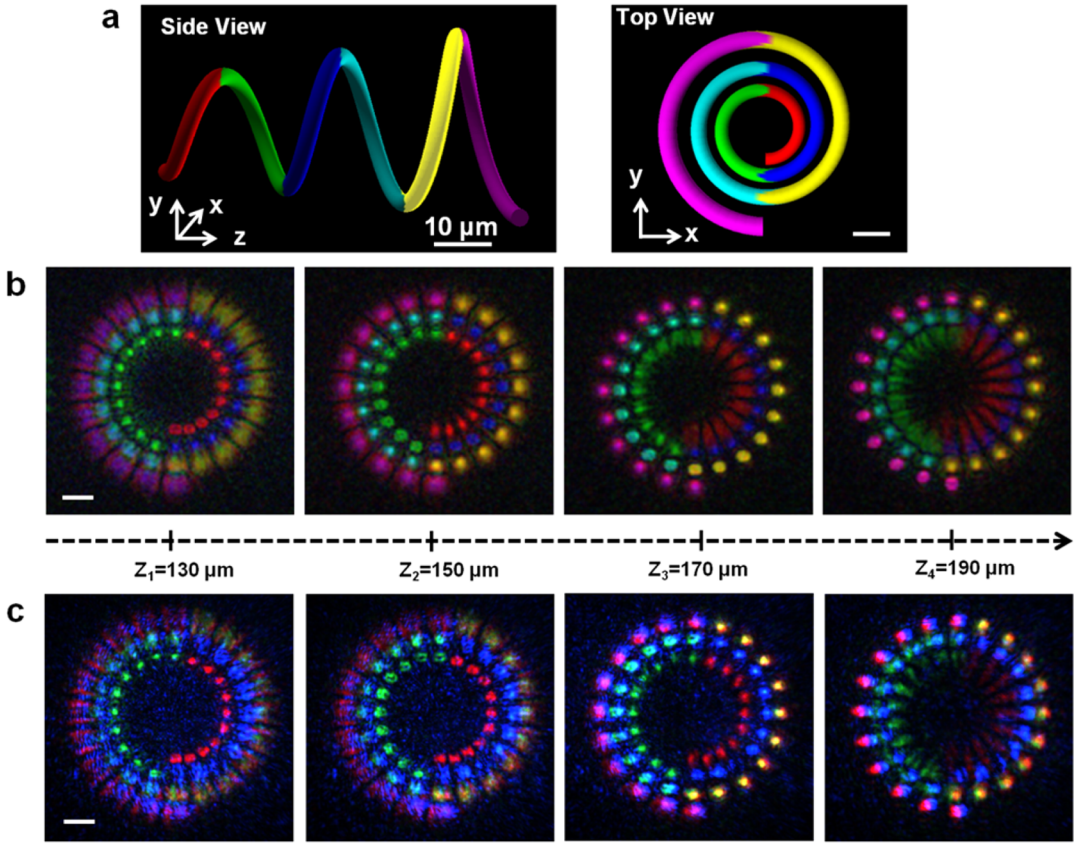

Figure 6. Reconstruction of 3D full-color holographic images for a color helix. (a) Side view and top view of the color helix. (b) Simulated on-axis evolution of the holographic images of the color helix on four 2D planes along *z* direction. (c) Experimentally reconstructed 3D holographic images on different 2D planes. All the scale bars indicate 10 *μ*m.

The unique advantages of the designed color meta-holograms with both amplitude and phase modulations enable the creation of vivid full-color holographic images with complex imaging patterns, as shown in Figure 5. The original 2D objects ("CMYW" letters and apple) in Figure 5a,d,g contain not only three primary colors (RGB) but also their secondary colors

DOI: 10.1021/acsnano.6b05453
ACS Nano 2016, 10, 10671−10680

(CMYW). Both the simulated (Figure 5b,e,h) and measured (Figure 5c,f,i) holographic images reconstructed from meta-holograms show great fidelity with the color, shape, and size of the original objects. Various secondary colors including but not limited to the cyan, magenta, and yellow colors have been successfully reproduced, as well as the white color where all three primary colors overlap to each other. For full-color holography, the adjustment of the white color balance is important for reproducing the natural color of an object, and it can be realized by carefully controlling the incident optical power of lasers. These experimental results also indicate the accurate spatial control of the reconstructed image pixels with different color components. Yet, there is still some background noise in the simulated holographic images and the experimentally reconstructed holographic images, compared to the original color objects in Figure 5. It is noted that the background noise is resulted from the modulations of amplitude and phase with the limited levels, rather than the superposition of the complex amplitudes of different colors components.

The meta-holograms can also be designed for the reconstruction of 3D color holographic images. As shown in Figure 6a, the original 3D object is a three-turn hollow helix pattern containing six different colors of RGB and CYM, with 20 μm pitch and gradually increased diameters from 15 to 33 μm. The helix axis is along z direction (perpendicular to the hologram plane). The reconstruction of the 3D color helix image on four 2D planes is simulated (Figure 6b) and measured (Figure 6c) at different distances relative to the meta-hologram. For z_1 = 130 μm above the hologram plane, only the red bottom part of the helix is in focus, whereas other parts of the helix are out of focus and appear blurry. As the z distance increases, each middle part of the helix with the certain color can form sharp images and finally the magenta top part is well focused around z_4 = 190 μm. As a result, the 3D full-color holographic image of the helix pattern has been successfully reconstructed. More demonstrations of 3D full-color holography for other objects using our designed meta-holograms with both amplitude and phase modulations can be found in Supporting Information Figures S6 and S7.

CONCLUSION

We have successfully demonstrated full-color ultrathin plasmonic metasurface holograms with both amplitude and phase modulations for the reconstruction of both 2D and 3D holographic images. The speckle noise is well suppressed by using the two-level amplitude modulation and eight-level phase modulation. By properly designing the encoded phase shifts, the incident angles of light, and the NA of objective lens, the generated meta-holograms are able to accurately reproduce the desired full-color holographic images with high quality. Since the plasmonic nanoslit unit cell is in subwavelength scale with only the fundamental mode supported, the metasurface holograms will not suffer from the ghost images produced by the high-order diffractions. Our demonstrated metasurface holograms have the advantages of achieving clean and vivid full-color holographic images with high resolution and low noise. Although we only consider the two-level amplitude modulation as the demonstration here, it is believed that the image quality could be further improved by involving more amplitude modulation levels. Note that the overall cross-polarization transmission of visible light from the currently designed nanoslit is only about 2%. A higher conversion efficiency from the metasurface can be achieved by using low-loss dielectric materials.[6,36−43] The current proof-of-concept approach in realizing transmission-type full-color metasurface holograms could also be easily extended to the reflection-type holograms with much higher conversion efficiency.[26] Further exploration of full-color metasurface holograms will enable the generation of more compact, efficient, and versatile wavelength-multiplexed planar optical devices for many holographic applications in optical imaging, beam shaping, optical information processing, and data storage.

METHODS

Wavelength-Multiplexed Encoding Method. A 2D object is placed at the object plane (x_0, y_0, z_0), and its complex field can be divided into three components $U_{0i}(x_0, y_0, z_0)$, where i = 1, 2 or 3, corresponding to red, green, or blue components. The hologram is placed at a plane (x, y, z), with a distance $d = z - z_0$ from the object plane. Based on the Huygens-Fresnel principle, the diffraction patterns of each color component on the hologram plane can be described by the Fresnel−Kirchhoff integral when the light incident angle is small[44,45]

$$U_i(x, y, z) = \frac{1}{j\lambda_i}\iint U_{0i}(x_0, y_0, z_0)\frac{\exp(jk_i\rho)}{\rho}\mathrm{d}x_0\mathrm{d}y_0$$

where $\rho = \sqrt{(x - x_0)^2 + (y - y_0)^2 + d^2}$ indicates the distance between two points on the object plane and the hologram plane. $k_i = 2\pi/\lambda_i$ is the wavevector. Since the reconstruction wavelength λ_i is quite small compared with the hologram dimension and the distance d (~100 μm), we can apply the Fresnel approximation and get the Fresnel diffraction formula

$$\begin{aligned} U_i(x, y, z) &= \frac{\exp(jk_id)}{j\lambda_id}\exp\left[\frac{jk_i}{2d}(x^2 + y^2)\right] \\ &\quad \iint U_{0i}(x_0, y_0, z_0)\exp\left[\frac{jk_i}{2d}(x_0^2 + y_0^2)\right] \\ &\quad \exp\left[-j\frac{2\pi}{\lambda_id}(xx_0 + yy_0)\right]\mathrm{d}x_0\mathrm{d}y_0 \\ &= \frac{\exp(jk_id)}{j\lambda_id}\exp\left[\frac{jk_i}{2d}(x^2 + y^2)\right] \\ &\quad F\left\{U_{0i}(x_0, y_0, z_0)\exp\left[\frac{jk_i}{2d}(x_0^2 + y_0^2)\right]\right\} \end{aligned}$$

where F represents the Fourier transform operation. U_i is the complex amplitude and can be written as $U_i(x,y,z) = A_i(x,y,z)\exp(j\varphi_i(x,y,z))$. Then an addition phase shift $\Delta\Phi_i$ along x direction is encoded into each U_i, and the final complex amplitudes of all the three color components are synthesized as

$$\begin{aligned} H(x, y, z) &= \sum_{i=1}^{3} U_i(x, y, z)\exp(j\Delta\Phi_i) \\ &= \sum_{i=1}^{3} A_i(x, y, z)\exp(j\varphi_i(x, y, z) - k_ix\sin\theta_i) \end{aligned}$$

The reconstructed light of RGB colors can be written as $R_i = \exp(k_ix\sin\theta_i)$. The reconstructed optical field distribution near the hologram is then given by

DOI: 10.1021/acsnano.6b05453
ACS Nano 2016, 10, 10671−10680

$$O(x, y, z) = H(x, y, z) \sum_{i=1}^{3} R_i = \sum_{i=1}^{3} A_i(x, y, z) \exp(j\varphi_i(x, y, z)) + \sum_{i=1, n=1, n\neq i}^{3} A_i(x, y, z)\exp(j\varphi_i(x, y, z) - k_i x\sin\theta_i + k_n x\sin\theta_n)$$

where the first term carries the information on the desired holographic images, and it can be separated from the second term (the unwanted image patterns) in both space and frequency domain.

This approach could be easily extended to reconstruct a complex full-color 3D object which could be divided into multiple 2D slices. It is noted that the cross-talk would be introduced and the quality of the reconstruction will be degraded when more slices are utilized to decompose the 3D object. However, it could be improved by considering the occlusion nulling.[46] For the reconstruction processes, the holographic images are calculated by replacing each pixel on the CGHs by a point source with corresponding amplitude and phase. All the simulations of holograms and reconstructed holographic images are carried out by the Matlab software.

Zero-Padding Technique. In order to make the pixel size of the color hologram independent of wavelengths, the relationship between the sampling numbers ($M \times N$) and the corresponding wavelengths for the RGB components should be satisfied as $M_R{:}M_G{:}M_B = N_R{:}N_G{:}N_B = \lambda_R{:}\lambda_G{:}\lambda_B$, indicating that a larger number of sampling points is needed for the longer wavelength. We set the sampling number of an object for RGB components as 512 × 512, 430 × 430, 340 × 340 pixels, respectively. The redundant marginal districts in the G-CGH and B-CGH are padded with zeros, thus the three-component holograms have the same pixel number of 512 × 512 and can be synthesized into one hologram. The zero-padding technique should also be applied to the numerical reconstruction, in order to make the pixel size of the reconstructed image independent of wavelengths. The sampling number of the wavelength-multiplexed hologram is set as 772 × 772, 648 × 648, and 512 × 512 pixels for red, green, and blue light. The redundant marginal districts in the diffraction patterns of green and blue light are padded with zeros to have the same pixel number as that of red light. Then, three images of red, green and blue colors with the same dimensions are superimposed to generate one combined full-color image.

Numerical Simulations. The plasmonic nanoslit unit cell is designed and simulated by using the finite integration time domain (FITD) solver of the CST Microwave Studio software. In the simulation, a circular polarized light is normally incident to the nanoslit from the side of the glass substrate. Periodic boundary conditions are employed along both the x and y axes in the nanoslit unit cell. Experimentally measured permittivity of aluminum[47] is used in the simulation, where the imaginary part is multiplied by a factor of 5 to take into account the surface irregularities and additional losses induced by the fabrication process. The refractive index of the glass substrate is set as 1.7. All sharp corners of the nanoslits are smoothened out by cylindrical surfaces with a radius of 30 nm in order to avoid unphysical structural discontinuities, mimicking the nanoslit fabrication condition.

Optical Setup. A color holographic image can be reconstructed by simultaneously illuminating the metasurface hologram with laser light of RGB colors in a tilted incident angle illumination configuration. Supporting Information Figure S4 shows the schematic of the optical measurement setup for characterizing the fabricated metasurface holograms. We employed three lasers at the wavelengths of 633 nm (red), 532 nm (green), and 420 nm (blue) with controlled incident angles of 35°, 0°, and −35°, respectively. Uniform optical illumination is ensured due to the small sizes of metasurface holograms. A linear polarizer (LP) and a quarter-wave plate (QWP) are utilized to create the desired circularly polarized light. The sample is mounted on the microscope stage with the metasurface hologram facing to the objective lens. An optical microscope with a 20× objective lens with NA = 0.4 is used to collect the transmission intensity from the metasurface hologram. A second LP and QWP pair is positioned in front of a charge-coupled device (CCD) camera in order to only capture the transmitted light with the opposite handedness.

The transmission spectrum (solid red curve in Figure 2d) from the uniform nanoslit array is measured with another home-built optical system similar to the setup shown in Supporting Information Figure S4, but using a halogen light source and a fiber-coupled optical spectrometer (LR1, ASEQ instruments). The overall cross-polarization transmission of the visible light is about 2%. A higher conversion efficiency from the metasurface can be achieved through further optimization of the nanoslit unit cell design, for example, by increasing the filling ratio of nanoslits, replacing high-loss metallic materials with low-loss dielectric materials, and using the three-layer reflection-type configuration.

ASSOCIATED CONTENT

Supporting Information

The Supporting Information is available free of charge on the ACS Publications website at DOI: 10.1021/acsnano.6b05453.

Refraction angle controlled by gradient phase, simulated cross-polarization transmission spectra and amplitude deviation with various nanoslit orientation angles, cross-polarization and copolarization transmission spectra and electric field distributions of nanoslit unit cell, experimental optical setup, simulated color holographic image for phase-only hologram, and reconstruction of 3D full-color holographic images for other objects (PDF)

AUTHOR INFORMATION

Corresponding Authors

*E-mail: gaojie@mst.edu

*E-mail: yangxia@mst.edu.

Notes

The authors declare no competing financial interest.

ACKNOWLEDGMENTS

The authors acknowledge support from the Office of Naval Research under Grant N00014-16-1-2408 and the National Science Foundation under Grant DMR-1552871. The authors also thank D. Rosenmann and D. A. Czaplewski at the Argonne National Laboratory for the aluminum thin film deposition. This work was performed, in part, at the Center for Nanoscale Materials, a U.S. Department of Energy, Office of Science, Office of Basic Energy Sciences User Facility under Contract No. DE-AC02-06CH11357.

DOI: 10.1021/acsnano.6b05453
ACS Nano 2016, 10, 10671−10680

REFERENCES

(1) Gabor, D. A. New Microscopic Principle. *Nature* **1948**, *161*, 777−778.
(2) Yu, N.; Genevet, P.; Kats, M. A.; Aieta, F.; Tetienne, J.; Capasso, F.; Gaburro, Z. Light Propagation with Phase Discontinuities: Generalized Laws of Reflection and Refraction. *Science* **2011**, *334*, 333−337.
(3) Ni, X.; Emani, N. K.; Kildishev, A. V.; Boltasseva, A.; Shalaev, V. M. Broadband Light Bending with Plasmonic Nanoantennas. *Science* **2012**, *335*, 427.
(4) Lin, J.; Mueller, J. P. B.; Wang, Q.; Yuan, G.; Antoniou, N.; Yuan, X.; Capasso, F. Polarization-Controlled Tunable Directional Coupling of Surface Plasmon Polaritons. *Science* **2013**, *340*, 331−334.
(5) Yin, X.; Ye, Z.; Rho, J.; Wang, Y.; Zhang, X. Photonic Spin Hall Effect at Metasurfaces. *Science* **2013**, *339*, 1405−1407.
(6) Lin, D.; Fan, P.; Hasman, E.; Brongersma, M. L. Dielectric Gradient Metasurface Optical Elements. *Science* **2014**, *345*, 298−302.
(7) Chen, X.; Huang, L.; Mühlenbernd, H.; Li, G.; Bai, B.; Tan, Q.; Jin, G.; Qiu, C.; Zhang, S.; Zentgraf, T. Dual-Polarity Plasmonic Metalens for Visible Light. *Nat. Commun.* **2012**, *3*, 1198.
(8) Yu, N.; Capasso, F. Flat Optics with Designer Metasurfaces. *Nat. Mater.* **2014**, *13*, 139−150.
(9) Kildishev, A. V.; Boltasseva, A.; Shalaev, V. M. Planar Photonics with Metasurfaces. *Science* **2013**, *339*, 1232009.
(10) Sun, S.; He, Q.; Xiao, S.; Xu, Q.; Li, X.; Zhou, L. Gradient-Index Meta-Surfaces as a Bridge Linking Propagating Waves and Surface Waves. *Nat. Mater.* **2012**, *11*, 426−431.
(11) Karimi, E.; Schulz, S. A.; De Leon, I.; Qassim, H.; Upham, J.; Boyd, R. W. Generating Optical Orbital Angular Momentum at Visible Wavelengths Using a Plasmonic Metasurface. *Light: Sci. Appl.* **2014**, *3*, e167.
(12) Lin, J.; Genevet, P.; Kats, M. A.; Antoniou, N.; Capasso, F. Nanostructured Holograms for Broadband Manipulation of Vector Beams. *Nano Lett.* **2013**, *13*, 4269−4274.
(13) Huang, L.; Chen, X.; Mühlenbernd, H.; Li, G.; Bai, B.; Tan, Q.; Jin, G.; Zentgraf, T.; Zhang, S. Dispersionless Phase Discontinuities for Controlling Light Propagation. *Nano Lett.* **2012**, *12*, 5750−5755.
(14) Zeng, J.; Gao, J.; Luk, T. S.; Litchinitser, N. M.; Yang, X. Structuring Light by Concentric-Ring Patterned Magnetic Metamaterial Cavities. *Nano Lett.* **2015**, *15*, 5363−5368.
(15) Zeng, J.; Li, L.; Yang, X.; Gao, J. Generating and Separating Twisted Light by Gradient-Rotation Split-Ring Antenna Metasurfaces. *Nano Lett.* **2016**, *16*, 3101−3108.
(16) Yu, N.; Aieta, F.; Genevet, P.; Kats, M. A.; Gaburro, Z.; Capasso, F. A Broadband, Background-Free Quarter-Wave Plate Based on Plasmonic Metasurfaces. *Nano Lett.* **2012**, *12*, 6328−6333.
(17) Pors, A.; Nielsen, M. G.; Bozhevolnyi, S. I. Broadband Plasmonic Half-Wave Plates in Reflection. *Opt. Lett.* **2013**, *38*, 513−515.
(18) Jiang, S.; Xiong, X.; Hu, Y.; Hu, Y.; Ma, G.; Peng, R.; Sun, C.; Wang, M. Controlling the Polarization State of Light with a Dispersion-Free Metastructure. *Phys. Rev. X* **2014**, *4*, 021026.
(19) Zhao, Y.; Alù, A. Tailoring the Dispersion of Plasmonic Nanorods to Realize Broadband Optical Meta-Waveplates. *Nano Lett.* **2013**, *13*, 1086−1091.
(20) Aieta, F.; Genevet, P.; Kats, M. A.; Yu, N.; Blanchard, R.; Gaburro, Z.; Capasso, F. Aberration-Free Ultrathin Flat Lenses and Axicons at Telecom Wavelengths Based on Plasmonic Metasurfaces. *Nano Lett.* **2012**, *12*, 4932−4936.
(21) Ni, X.; Ishii, S.; Kildishev, A. V.; Shalaev, V. M. Ultra-Thin, Planar, Babinet-Inverted Plasmonic Metalenses. *Light: Sci. Appl.* **2013**, *2*, e72.
(22) Shitrit, N.; Yulevich, I.; Maguid, E.; Ozeri, D.; Veksler, D.; Kleiner, V.; Hasman, E. Spin-Optical Metamaterial Route to Spin-Controlled Photonics. *Science* **2013**, *340*, 724−726.
(23) Huang, L.; Chen, X.; Mühlenbernd, H.; Zhang, H.; Chen, S.; Bai, B.; Tan, Q.; Jin, G.; Cheah, K.; Qiu, C.; Li, J.; Zentgraf, T.; Zhang, S. Three-Dimensional Optical Holography Using a Plasmonic Metasurface. *Nat. Commun.* **2013**, *4*, 2808.
(24) Ozaki, M.; Kato, J.; Kawata, S. Surface-Plasmon Holography with White-Light Illumination. *Science* **2011**, *332*, 218−220.
(25) Ni, X.; Kildishev, A. V.; Shalaev, V. M. Metasurface Holograms for Visible Light. *Nat. Commun.* **2013**, *4*, 2807.
(26) Zheng, G.; Mühlenbernd, H.; Kenney, M.; Li, G.; Zentgraf, T.; Zhang, S. Metasurface Holograms Reaching 80% Efficiency. *Nat. Nanotechnol.* **2015**, *10*, 308−312.
(27) Montelongo, Y.; Tenorio-Pearl, J. O.; Williams, C.; Zhang, S.; Milne, W. I.; Wilkinson, T. D. Plasmonic Nanoparticle Scattering for Color Holograms. *Proc. Natl. Acad. Sci. U. S. A.* **2014**, *111*, 12679−12683.
(28) Walther, B.; Helgert, C.; Rockstuhl, C.; Setzpfandt, F.; Eilenberger, F.; Kley, E.; Lederer, F.; Tünnermann, A.; Pertsch, T. Spatial and Spectral Light Shaping with Metamaterials. *Adv. Mater.* **2012**, *24*, 6300−6304.
(29) Huang, Y.; Chen, W. T.; Tsai, W.; Wu, P. C.; Wang, C.; Sun, G.; Tsai, D. P. Aluminum Plasmonic Multicolor Meta-Hologram. *Nano Lett.* **2015**, *15*, 3122−3127.
(30) Xue, G.; Liu, J.; Li, X.; Jia, J.; Zhang, Z.; Hu, B.; Wang, Y. Multiplexing Encoding Method for Full-Color Dynamic 3D Holographic Display. *Opt. Express* **2014**, *22*, 18473−18482.
(31) Li, X.; Ren, H.; Chen, X.; Liu, J.; Li, Q.; Li, C.; Xue, G.; Jia, J.; Cao, L.; Sahu, A.; Hu, B.; Wang, Y.; Jin, G.; Gu, M. Athermally Photoreduced Graphene Oxides for Three-Dimensional Holographic Images. *Nat. Commun.* **2015**, *6*, 6984.
(32) Bomzon, Z.; Biener, G.; Kleiner, V.; Hasman, E. Space-Variant Pancharatnam−Berry Phase Optical Elements with Computer-Generated Subwavelength Gratings. *Opt. Lett.* **2002**, *27*, 1141−1143.
(33) Bomzon, Z.; Kleiner, V.; Hasman, E. Pancharatnam−Berry Phase in Space-Variant Polarization-State Manipulations with Subwavelength Gratings. *Opt. Lett.* **2001**, *26*, 1424−1426.
(34) Zhao, J.; Jiang, H.; Di, J. Recording and Reconstruction of a Color Holographic Image by Using Digital Lensless Fourier Transform Holography. *Opt. Express* **2008**, *16*, 2514−2519.
(35) Zheng, H.; Wang, T.; Dai, L.; Yu, Y. Holographic Imaging of Full-Color Real-Existing Three-Dimensional Objects with Computer-Generated Sequential Kinoforms. *Chin. Opt. Lett.* **2011**, *9*, 040901−40904.
(36) Khorasaninejad, M.; Ambrosio, A.; Kanhaiya, P.; Capasso, F. Broadband and Chiral Binary Dielectric Meta-Holograms. *Science Advances* **2016**, *2*, e1501258.
(37) Khorasaninejad, M.; Chen, W. T.; Zhu, A. Y.; Oh, J.; Devlin, R. C.; Rousso, D.; Capasso, F. Multispectral Chiral Imaging with a Metalens. *Nano Lett.* **2016**, *16*, 4595−4600.
(38) Huang, K.; Dong, Z.; Mei, S.; Zhang, L.; Liu, Y.; Liu, H.; Zhu, H.; Teng, J.; Luk'yanchuk, B.; Yang, J. K. W.; Qiu, C. Silicon Multi-Meta-holograms for the Broadband Visible Light. *Laser Photon. Rev.* **2016**, *10*, 500−509.
(39) Arbabi, A.; Horie, Y.; Bagheri, M.; Faraon, A. Dieletric Metasurface for Complete Control of Phase and Polarization with Subwavelength Spatial Resolution and High Transmission. *Nat. Nanotechnol.* **2015**, *10*, 937−943.
(40) Zhao, W.; Liu, B.; Jiang, H.; Song, J.; Pei, Y.; Jiang, Y. Full-Color Hologram Using Spatial Multiplexing of Dielectric Metasurface. *Opt. Lett.* **2016**, *41*, 147−150.
(41) Zhao, W.; Jiang, H.; Liu, B.; Song, J.; Jiang, Y.; Tang, C.; Li, J. Dielectric Huygen's Metasurface for High-Efficiency Hologram Operating in Transmission Mode. *Sci. Rep.* **2016**, *6*, 30613.
(42) Wang, B.; Dong, F.; Li, Q.; Yang, D.; Sun, C.; Chen, J.; Song, Z.; Xu, L.; Chu, W.; Xiao, Y.; Gong, Q.; Li, Y. Visible-Frequency Dielectric Metasurfaces for Multiwavelength Achromatic and Highly Dispersive Holograms. *Nano Lett.* **2016**, *16*, 5235−5240.
(43) Devlin, R. C.; Khorasaninejad, M.; Chen, W.; Oh, J.; Capasso, F. High Efficiency Dielectric Metasurfaces at Visible Wavelengths. 2016, *arXiv:1603.02735*. arXiv.org e-Print archive. http://arxiv.org/abs/1603.02735 (accessed July 2016).
(44) Picart, P.; Li, J. *Digital Holography*; Wiley-ISTE: Hoboken, NJ, 2012.

DOI: 10.1021/acsnano.6b05453
ACS Nano 2016, 10, 10671−10680

(45) Schnars, U.; Falldorf, C.; Watson, J.; Jüptner, W. *Digital Holography and Wavefront Sensing*; Springer: New York, 2015.
(46) Wakunami, K.; Yamashita, H.; Yamaguchi, M. Occlusion Culling for Computer Generated Hologram Based on Ray-Wavefront Conversion. *Opt. Express* **2013**, *21*, 21811−21822.
(47) Palik, E. D. *Handbook of Optical Constants of Solids*; Academic Press: Waltham, MA, 1985; Vol. *1*.

NOTE ADDED AFTER ASAP PUBLICATION

Figure 5, the abstract figure, and typos were amended after ASAP publication on September 26, 2016. The article was reposted ASAP November 16, 2016.

DOI: 10.1021/acsnano.6b05453
ACS Nano 2016, 10, 10671−10680